MULTISCALE MODEL. SIMUL.
Vol. 12, No. 1, pp. 181–199

APPROXIMATING OFF-LATTICE KINETIC MONTE CARLO*

HENRY A. BOATENG†, TIM P. SCHULZE‡, AND PETER SMEREKA†

Abstract. We present an approximate off-lattice kinetic Monte Carlo (KMC) method for simulating heteroepitaxial growth. The model aims to retain the speed and simplicity of lattice based KMC methods while capturing essential features that can arise in an off-lattice setting. Interactions between atoms are defined by an interatomic potential which determines the arrangement of the atoms. In this formulation we assign rates for configuration changes that are keyed to individual surface atoms in a fashion similar to bond-counting schemes. The method is validated by simulations of heteroepitaxial growth, annealing of strained bilayer systems, and a qualitative verification of Stoney's formula. The algorithm captures the effects of misfit on the growth modes, anticorrelation of quantum dots grown on both sides of a substrate, the effects of deposition flux on island size, the formation of edge dislocations to relieve strain, and naturally incorporates intermixing.

Key words. off-lattice, kinetic Monte Carlo, heteroepitaxy, crystal growth, dislocations

AMS subject classifications. 82B80, 65Z99, 70-08

DOI. 10.1137/130927528

1. Introduction.

This paper is aimed at simulating heteroepitaxy. To this end we introduce an approximate implementation of an off-lattice kinetic Monte Carlo (KMC) method. For the simulations, we have in mind typical length scales are approaching a micron and time scales are on the order of seconds. Even with great advances in accelerated molecular dynamics (MD) methods [32, 31, 33, 34, 30], it is evident that MD simulations on these scales are impossible for the foreseeable future. Closely related to MD and, in principle, nearly as faithful to the underlying physics, are off-lattice KMC methods. In a sense, these are the ultimate accelerated MD methods, but they are still too slow for simulations on the desired length and time scales. For these reasons, most modeling and simulation of heterostructured nanomaterials has been done via continuum mechanics.

In contrast, simulation of the growth and evolution of pure crystals (e.g., homoepitaxy) at the nanoscale is dominated by lattice based KMC. While most KMC simulations are lattice based, many of the important technological applications involve multicomponent systems where lattice mismatch leads to elastic strain, one of several reasons off-lattice effects may be important. Incorporating elastic effects into KMC simulations in a way that retains the simplicity and speed of the basic method has emerged as a central challenge. This work is aimed at addressing this challenge.

The present method is quite different from self-learning and other off-lattice KMC methods. Ideally, it seeks to have the same state space, but the rates are more in the spirit of lattice based, bond-counting methods than methods based on probing energy landscapes for transition paths. There is no exhaustive catalog of events, but rather rates are computed on the fly in a fast, but simplified, way and are tied to atoms in a

*Received by the editors July 3, 2013; accepted for publication (in revised form) November 25, 2013; published electronically February 6, 2014. This work was supported in part by NSF FRG grant DMS 0854870.

http://www.siam.org/journals/mms/12-1/92752.html

†Department of Mathematics, University of Michigan, Ann Arbor, MI 48109-1109 (boateng@umich.edu, psmereka@umich.edu). The third author was supported in part by NSF grant DMS-1115252.

‡Department of Mathematics, University of Tennessee, Knoxville, TN 37996-1300 (schulze@math.utk.edu).

way that mimics many of the basic features of bond-counting schemes, e.g., detailed balance and dependence on the local environment. The limitations are that the model is approximate, capturing a fair amount of physics in the same way that lattice based bond-counting models do, but ultimately having nowhere near the level of accuracy (assuming the empirical potential and transition state theory hold) of fully off-lattice KMC methods. The advantage is that it is much faster and simpler to implement, allowing one to study much larger systems over much longer time scales.

1.1. Off-lattice kinetic Monte Carlo. The rationale for off-lattice KMC simulation of crystal growth is based on observations of MD simulations and an approximate model of those simulations based on transition state theory (TST) [14, 12, 13, 19, 4, 20, 11]. The essence of this model is that the system spends most of its time randomly oscillating within the N-particle, dN-dimensional configuration space about a local minimizer $x_m \in \mathbb{R}^{dN}$ of the system potential energy, $U(x)$, with rare transitions between these basins of attraction. For the system to transition from basin i to basin j, it has to overcome a minimum energy barrier ΔU_{ij}. If k_BT is the energy scale defined by the temperature of the film, then the harmonic approximation to TST estimates the rate R_{ij} at which the transition from basin i to basin j occurs as

$$R_{ij} = K \exp(-\Delta U_{ij}/k_BT), \tag{1.1}$$

where $K(T)$ is a weakly temperature-dependent attempt rate.

These observations suggest an alternative model where the Newtonian dynamics is replaced by a Markov-chain, with the system making relatively rare, random transitions between states X_i that represent local minimizers in the system's configuration space at rates R_{ij} calculated from (1.1). More specifically the energy barrier,

$$\Delta U = U(x_s) - U(x_m), \tag{1.2}$$

requires locating both the initial local minimum, x_m, and the saddle point, x_s (where $\nabla U = 0$ and all but one of the principal curvatures are positive), separating the basins of attraction. Note that these local minima and saddle points are, in principle, determined by the motion of all of the particles simultaneously within the configuration space. When this sort of scheme is carried out in detail, it is referred to as off-lattice KMC or on-the-fly KMC [14, 12, 13, 19, 4, 20, 11]. While this is much faster than the corresponding MD simulation, or even accelerated MD simulations based on similar considerations [32, 31, 33, 34, 30], it is still prohibitively expensive in that one could not hope to simulate the growth of a crystal on physically relevant space and time scales. Furthermore, this type of model is somewhat difficult to implement, requiring, for each and every transition, an exhaustive search for saddle points within the dN-dimensional configuration space. This level of generality allows the model to capture complex, multiatom transitions.

Monte Carlo simulations of crystal growth and diffusion on strained surfaces employing a continuous space potential have been in use for a while [7, 24]. In particular there have been previous KMC studies of heteroepitaxy modeled with a Lennard-Jones pair interaction potential [19, 4, 20]. The main difference in our work from the approach of [19, 4, 20] is in how the rates are computed. The work in [19, 4, 20] employs a *frozen crystal approximation* in $1+1$-dimensions, where the saddle points are the maxima of the potential energy surface produced by moving each surface atom while freezing all other atoms. The *frozen crystal approximation* offers computational speedup since the problem of detecting saddle points becomes essentially a one particle problem.

1.2. On-lattice kinetic Monte Carlo. For single-crystal, homoepitaxial systems, an often-used and greatly simplified model immediately suggests itself [17, 6, 29]. In the simplified approach, the states are approximated using occupation arrays structured in the form of a perfect lattice—most often simple cubic, but face centered cubic (fcc) and other lattices are also used; the allowed transitions are restricted to a limited catalog of characteristic events, and the transition rates are parameterized based on the local lattice configuration. Indeed, it is this type of model that people generally refer to when they speak of KMC. In the vast majority of these models, an important simplification is the restriction of the transition catalog to single-particle moves. In this context, it is often simpler to label the rates using a single index i that refers to the hopping atom, and we will adopt this notation from this point on. For example,

$$R_i = mK \exp\left(-\gamma n_i / k_B T\right), \tag{1.3}$$

where n_i is the number of nearest-neighbor bonds that are broken by a single-particle transition, i.e., "hop," m is the number of destinations for the hop, and γ is the bond energy. While this model is idealized, it captures the essential physical effects of homoepitaxial growth, such as surface diffusion and nucleation. Furthermore, the model satisfies detailed balance, which implies that, in the absence of deposition, the model will approach a Boltzmann distribution. Notice that the rates for this model are independent of the particle's destination; there exist many variations on this model that account for such non–nearest-neighbor effects. Finally, it is important to realize that bond-counting KMC is orders of magnitude faster than off-lattice KMC, a gap in performance we seek to bridge by introducing intermediate approximations.

1.3. Weakly off-lattice kinetic Monte Carlo. Bond-counting models are inappropriate when the basins of attraction are modified by long-range elastic deformation. In particular, the elastic strain due to misfit in heteroepitaxy falls into this category. Orr et al. [21], Lam, Lee, and Sander [16], and Lung, Lam, and Sander [18] have proposed a modification of the bond-counting model (1.3) where the discrete configurations of the lattice based model are supplemented by a ball-and-spring model for elastic interactions. Thus, there is a displacement field associated with each discrete configuration that determines the elastic contribution to the total energy. The hopping rate is taken to be

$$R_i = mK \exp[(-n_i\gamma + \Delta W_i)/(k_B T)], \tag{1.4}$$

where ΔW_i is the elastic correction to the energy barrier. This is given by

$$\Delta W_i = W - W^{(i)}, \tag{1.5}$$

where W is the total elastic energy in mechanical equilibrium and $W^{(i)}$ is the total elastic energy of the configuration in mechanical equilibrium with atom i removed.

In a bid to efficiently implement this model, multigrid methods with artificial boundary conditions have been developed to quickly solve for the elastic field [22, 23]. A speedup in the implementation of the model has been gained by finding accurate estimates on the elastic energy change in terms of the current configuration [25, 26]. As a result the elastic field need only be computed for the moving atoms. Additionally, an energy localization technique has been developed where the change in elastic energy can be accurately approximated using local computations [25, 26]. The approach of [25, 26] has been extended to allow for intermixing and used to simulate quantum dots as well as stacked quantum dots [2, 27].

2. Approximate off-lattice kinetic Monte Carlo. One drawback of the bond-counting models, including the weakly off-lattice model described above, is that they are based on a lattice and as such they cannot capture some important physical effects such as surface reconstructions and dislocations. Our model removes the constraint on the arrangement of the atoms by letting the atoms interact via an empirical potential. Our goal is to extend the weakly off-lattice KMC formulation to an off-lattice setting in a way that retains the computational advantages of the former model. Many of these advantages stem from restricting the model to single-particle moves and specifying the number of allowed destinations for each particle.

In the approximate two-dimensional model presented below we assume that events are associated with specific atoms, and each atom is associated with exactly two events, a hop to the left and a hop to the right. After the hop, the system is allowed to relax, which introduces the possibility for at least some concerted moves, including the formation of dislocations, and to handle regions where the lattice may not be coherent.

To proceed in this manner, we need a formula for the hopping rates. Our model is based on the observation that (1.4) can be written in the form

$$R_i = mK \exp[\Delta E_i/(k_B T)], \tag{2.1}$$

where ΔE_i represents the change in the total energy when removing the ith atom (i.e., $E - E^{(i)}$).

The idea behind this formulation is to retain the form of (2.1) but replace the energy of the weakly off-lattice model, E, with an energy given by an intermolecular potential, $U(x)$. For surface atom i we then take the hopping to be

$$R_i = mK \exp(\Delta U_i/k_B T), \tag{2.2}$$

where

$$\Delta U_i = U(x_m) - U(x_m^{(i)}), \tag{2.3}$$

x_m is the current configuration (a local minimizer), and $x_m^{(i)}$ is the configuration obtained by first removing atom i and then relaxing the configuration by a monotone descent method. Notice that unlike (1.5), this formula accounts for both the bond and (nonlinear) elastic energy. This approach retains the assumption that the hopping rate is independent of the atom's destination.

The algorithm satisfies detailed balance for the vast majority of moves but it cannot always be satisfied. This failure can happen when the relaxation step involves a large number of concerted moves, for example, when an atom hops and the resulting relaxation step results in the formation of a dislocation. Clearly, with our algorithm it is not possible, via a single-atom move, for the system to move back to the dislocation-free state. In reality we expect these events to be quite rare. Therefore, this algorithm violates detailed balance by essentially removing the possible occurrence of some very rare events.

We will consider the deposition of type A atoms on a type B substrate, with the atoms interacting via a Lennard-Jones potential [1, 8]. The equilibrium configurations are determined by relaxing the system. The total energy, U, of a system of N particles interacting by the Lennard-Jones potential is given by

$$U(x) = \sum_{i<j}^{N} \phi(r_{ij}), \quad \text{where } \phi(r_{ij}) = 4\epsilon_{ij}\left[\left(\frac{\sigma_{ij}}{r_{ij}}\right)^{12} - \left(\frac{\sigma_{ij}}{r_{ij}}\right)^{6}\right], \tag{2.4}$$

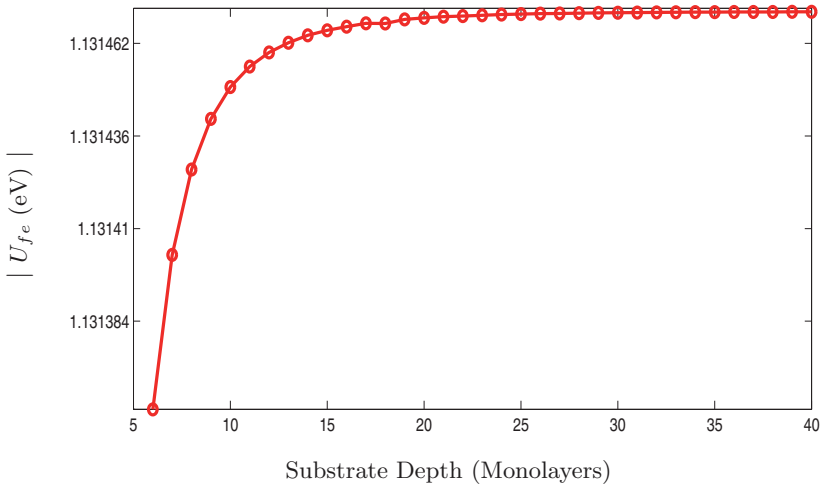

FIG. 1. *Film energy per atom versus substrate depth with misfit* $\eta = -0.04$. *The film energy per atom is approximately constant for substrates of depth* 30 *atoms or more.*

$x \in \mathbb{R}^{2N}$ is the current configuration in $(1+1)$-dimension, r_{ij} is the distance between atoms i and j, $\phi(r_{ij})$ is the interaction potential, σ_{ij} is the relaxed bond length, and ϵ_{ij} is the chemical bond energy. We use the Lorentz–Berthelot mixing rules [1, 8] and take

$$\sigma_{ij} = \begin{cases} \sigma_A & \text{if both atoms are type A,} \\ \sigma_B & \text{if both atoms are type B,} \\ \frac{1}{2}(\sigma_A + \sigma_B) & \text{if the atoms are different} \end{cases}$$

and

$$\epsilon_{ij} = \begin{cases} \epsilon_A & \text{if both atoms are type A,} \\ \epsilon_B & \text{if both atoms are type B,} \\ \sqrt{\epsilon_A \epsilon_B} & \text{if the atoms are different.} \end{cases}$$

We use $\epsilon_A = 0.3387$ eV for the deposited atoms and $\epsilon_B = 0.4$ eV for the substrate atoms. These are chosen to match the relative strengths of a Ge-Ge single bond to that of a Si-Si single bond, respectively. We take the lattice constant of the substrate, σ_B, to be 2.7153 Å, which matches the bond length of Silicon. The lattice constant of the deposited material, σ_A, depends on the misfit η, where

$$\eta = \frac{\sigma_B - \sigma_A}{\sigma_B}. \tag{2.5}$$

We truncate the potential at a cutoff radius $r_c = 4\sigma_B$; hence a particle at position x_i only interacts with particles that lie in a disk of radius $r_c = 4\sigma_A$ centered at x_i, and the cost of computing the potential is reduced from $O(N^2)$ to $O(N)$. At $r_c = 4\sigma_B$, the potential is approximately 1/1000th of the minimum. The system is modeled with periodic boundary conditions in the horizontal direction to suppress edge effects and has a substrate depth, h_s, of 40 monolayers to approximate an infinitely deep substrate. Figure 1 is a plot of the film energy per atom versus substrate depth for a bilayer system that is 256 atoms wide with four percent misfit. For a system with N_A substrate atoms and N_B film atoms, if U_{A+B} is the energy of the system and U_A is

the energy of the corresponding system of only N_A substrate atoms, the film energy per atom, U_{fe}, is approximated as

$$U_{fe} = \frac{U_{A+B} - U_A}{N_B}. \tag{2.6}$$

In Figure 1, the substrate depth $6 \leq h_s \leq 40$ and the film depth is fixed at 6. The film energy per atom is approximately constant for substrate depths $h_s \geq 30$ ML.

3. Implementation. Recall that the steps in a rejection-free KMC model with deposition are as follows:

1. Compute the hopping rates, $\{R_k\}_{k=1}^N$, for all N surface atoms, with $R_k = \omega e^{\Delta U/k_B T}$, where $\omega = mK = 10^{12} s^{-1}$.
2. Compute the partial sums $p_j = \sum_{k=1}^{j} R_k$.
3. Find the total rate for all processes, $R_{\text{total}} = R_d + \sum_{k=1}^{N} R_k$, where R_d is the rate of deposition.
4. Draw a random number $r \in (0, R_{\text{total}})$.
5. Hop the first surface atom for which $p_j > r$. If $r > p_N$, deposit an atom.
6. Go to step 1.

The main processes in KMC are deposition and surface hopping. Each of these potentially moves the system away from mechanical equilibrium. As a result, the system is relaxed after each event. We perform this relaxation of the system in two stages. First, the deposited atom or the adatom is drawn to the surface of the film by a steepest descent procedure. The atom feels forces from frozen atoms in a disk of radius $4\sigma_B$ centered at the atom. We use a cell linked-list [1, 8] in order to determine the atoms in the disk and the boundary atoms in $O(N)$ time. After this, the system is then relaxed using a nonlinear conjugate gradient method, which is detailed in the next subsection.

In principle, the system needs to be globally relaxed after each event. As a time saving measure, however, after most events we perform a local relaxation of all atoms that are at most a distance of $r_c = 4\sigma_B$ from the deposited or hopping atom. After a fixed number of events have transpired, we globally relax the system.

3.1. Determining positions for atoms. In this section we explain the procedure for the deposition and hopping of atoms. In our model, only surface atoms can hop. Surface atoms are defined as atoms with coordination number less than five, excluding the atoms in the bottom layer. We define the coordination number of an atom as the number of atoms lying within a radius of $1.2\sigma_B$, i.e., the nearest-neighbor atoms. A fully coordinated atom has a coordination number of six. It is fairly straightforward to determine the hopping positions in bond-counting KMC since the atoms are restricted to discrete lattice sites. The situation is different in our model since there is no restriction on the positions of the atom; as such, determining hopping positions is a challenge. To retain some of the simplicity of lattice based schemes, we are going to define a model where we move the atom to a randomly chosen, nearby position on the surface. Ideally one would like to choose randomly from nearby basins of attraction. In order to simplify this task we assume, as described below, that a single atom moves to a location determined by the assumption of a nearly coherent lattice.

The first step of this procedure identifies all surface atoms (those with four or fewer bonds) that are within $4\sigma_B$ of the hopping atom. One of these surface atoms is then chosen at random. We then compute $U(x)$ at the six vertices of a hexagon

centered on the chosen surface atom. The atom is initially placed at the vertex with the lowest energy, where it will be relaxed by the procedures described below. Picking the lowest energy site naturally avoids initially placing the atom too close to or too far from the other atoms.

The procedure for depositing an atom starts by generating its initial coordinates, (x_c, y_c), with x_c sampled from $U(0, L)$, where L is the width of the system. The y_c-coordinate is set to $y_{\max} + y_0$, where $y_{\max}$ is the maximum height of the configuration and y_0 is a fixed constant. Next, one checks whether or not there are any other atoms in a radius of $2\sigma_B$ centered at (x_c, y_c). If no atoms are found, then y_c is reduced by σ_B. This is repeated until atoms are present. At this point, the atom is now quite close to the surface and we apply a local relaxation which will incorporate the atom into the crystal. The deposition event is complete.

3.2. Relaxation with nonlinear conjugate gradient. After an atom hop or deposition event, the system is relaxed, either locally or globally, so that the system is in a new local minimum. To mimic realistic dynamics, one wants the system to move from one local minimum to a neighboring one. Therefore, after choosing one of the candidate moves outlined above, it is important that the minimization scheme follow a descent algorithm so that the system stays within the selected basin of attraction. We now describe the global relaxation scheme.

We use a nonlinear variant of the conjugate gradient method [28] as the relaxation routine and deem a configuration to be a local minimizer if the maximum norm of the force

$$\|\nabla U\|_\infty = \max_i \left| \frac{\partial U}{\partial x_i} \right| \leq 10^{-2}, \tag{3.1}$$

where x_i refers to the ith coordinate.

The conjugate gradient method proceeds iteratively by a series of line searches to find the minimum along conjugate directions. The method starts at the present configuration x_{old} and initially proceeds in the steepest descent direction, $r = -\nabla U$, which is also the first conjugate direction d. The minimum of $U(x)$ along this direction is located at

$$x_{\text{new}} = x_{\text{old}} + \alpha d, \tag{3.2}$$

where

$$\alpha = -\frac{\nabla U^T d}{d^T H d} \tag{3.3}$$

is obtained by a Newton–Raphson line search. Here, H is the $2N \times 2N$ Hessian matrix with components

$$H_{ij}^{mn} = \frac{\partial^2 U}{\partial x_i^m \partial x_j^n}, \tag{3.4}$$

where x_i^m is the m-coordinate of the ith atom and m refers to an x- or y-coordinate. For a pair potential of the form in (2.4),

$$\begin{aligned} \frac{\partial^2 U(r_{ij})}{\partial x_i^m \partial x_j^n} = \delta_{ij} \sum_{\substack{k=1 \\ k \neq i}}^{N} \left\{ \phi''(r_{ik}) \frac{\partial r_{ik}}{\partial x_k^n} \frac{\partial r_{ik}}{\partial x_i^m} + \phi'(r_{ik}) \frac{\partial^2 r_{ik}}{\partial x_k^n \partial x_i^m} \right\} \\ + (1 - \delta_{ij}) \left\{ \phi''(r_{ij}) \frac{\partial r_{ij}}{\partial x_j^n} \frac{\partial r_{ij}}{\partial x_i^m} + \phi'(r_{ij}) \frac{\partial^2 r_{ij}}{\partial x_j^n \partial x_i^m} \right\}, \end{aligned} \tag{3.5}$$

where r_{ij} is the distance between atom i and atom j.

The new conjugate search direction is computed from the new residual $r = -\nabla U$ and the present conjugate direction as

$$d = -\nabla U(x) + \beta d. \tag{3.6}$$

We use the Polak–Ribière formula [28],

$$\beta = \frac{r_{k+1}^T (r_{k+1} - r_k)}{r_k^T r_k}, \tag{3.7}$$

to find the step size, β. The algorithm is forced to use the steepest descent direction, that is, set $d = r$ or $\beta = 0$, under two conditions:

1 When $\beta < 0$, which means the new direction is close, but not conjugate, to the previous direction since the numerator of (3.7) is negative.
2 When $r^T d \leq 0$, which means that d is not a descent direction and that the algorithm has lost conjugacy.

With the new conjugate direction found, a new line search, i.e., computing α, is then performed to determine the new position and the process repeats.

A local relaxation is performed after every hop or deposition. The local region of relaxation is the adatom or the deposited atom and all the atoms that are at most a distance of $4\sigma_B$ away from it. The local relaxation algorithm has all the features of the global nonlinear conjugate gradient algorithm plus a backtracking algorithm. With backtracking, we check within each line search to ensure that the energy is decreasing and that none of the atoms in the new local configuration lie outside the local region of relaxation. Failure to meet these criteria indicates that the Newton step is too large, so we revert to the previous local configuration, halve the step size, and repeat the computation. This is repeated until the new configuration lies in the region of relaxation and is lower in energy than the previous configuration. Finally, the force on the boundary of the local region is monitored after each local relaxation, and if this force is larger than a threshold, a global relaxation is performed. This condition is triggered more often at higher misfits, where the strain in the system is larger.

3.3. Approximate rates. A major bottleneck in KMC with elastic effects is computing the hopping rates for each surface atom for every KMC step. This involves removing each surface atom and relaxing the full system or, worse, explicitly finding all the saddle points. In order to overcome this bottleneck, we adopt the approach of Schulze and Smereka [26], who have shown that the rates in the weakly off-lattice model can be estimated using a local energy approximation. The idea is to approximate ΔU (equation (2.3)) using a local quantity. To this end, we establish an empirical, linear relationship between a local distortion energy, which depends only on the nearest neighbors of the atom, and a global distortion energy, which depends on the whole system:

$$\Delta U - \Delta U_{\text{appx}} = C(\eta)(\Delta U^{\text{loc}} - \Delta U^{\text{loc}}_{\text{ideal}}). \tag{3.8}$$

Table 1 explains the terms used to establish the linear relationship. Figure 2 is a depiction of a representative system showing the bonds of one surface atom. The nearest-neighbor bonds are solid lines and the other bonds are dotted lines.

The definition of ΔU is given in (2.3), and we define ΔU_{appx} as the energy due to the interaction of the surface atom that is being moved with every other atom,

TABLE 1
Definitions for ΔU, ΔU_{appx}, ΔU^{loc}, and ΔU^{loc}_{ideal} based on Figure 2.

ΔU	Energy of A - energy of B relaxed
ΔU_{appx}	Energy in solid and dotted bonds
ΔU^{loc}	Energy in solid (nearest-neighbor) bonds
$\Delta U^{\text{loc}}_{\text{ideal}}$	Energy in solid bonds in ideal configuration

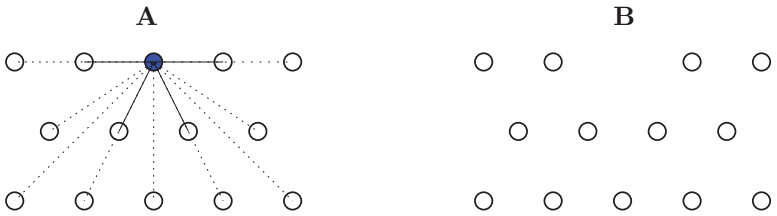

FIG. 2. **A** *is a relaxed configuration and* **B** *is the configuration with the colored surface atom removed. The solid lines are nearest-neighbor bonds and the dotted lines are bonds farther away.*

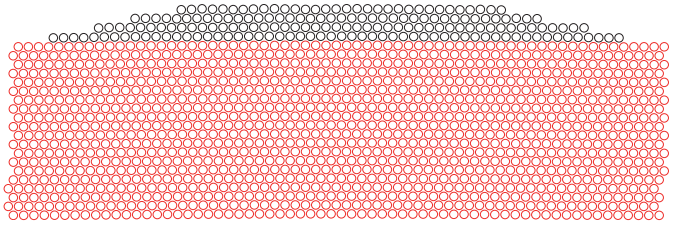

FIG. 3. *The configuration used to establish the linear relationship between the local and global distortions. The light (red) circles are the substrate atoms and the dark (black) circles are the film atoms.*

i.e., the energy needed to break all the bonds with this atom, but not accounting for any relaxation. We define ΔU^{loc} as the energy in the bonds that an atom forms with its nearest neighbors, i.e., the local energy change when the surface atom is removed. The quantity $\Delta U^{\text{loc}}_{\text{ideal}}$ is similar to ΔU^{loc} except the atom and its nearest neighbors are assumed to be in an ideal configuration; i.e., the energy between the atom i and any of its nearest neighbors j is $-\epsilon_{ij}$, the minimum of the Lennard-Jones potential for a pair interaction.

As pointed out in [26] one can establish an empirical relationship between the global change in elastic energy when removing an atom and the local elastic energy density. Following the same procedure, we compute the local and global distortions for the configuration shown in Figure 3 and fit a linear relationship between them for several values of the misfit as shown in Figure 4 (plots I–V). We establish a quadratic relationship between misfits and the slope of the best fit lines as shown in plot (VI) of Figure 4. Note that in the weakly off-lattice model, the slopes in the linear relationship between local and global energy differences are independent of misfit, whereas here the nonlinear nature of the empirical potential results in a misfit-dependent slope. This allows us to estimate ΔU and hence the rates for all the surface atoms quickly for any misfit we study.

In what follows, we use the approximate relationships established in this section in place of the computationally expensive global calculations.

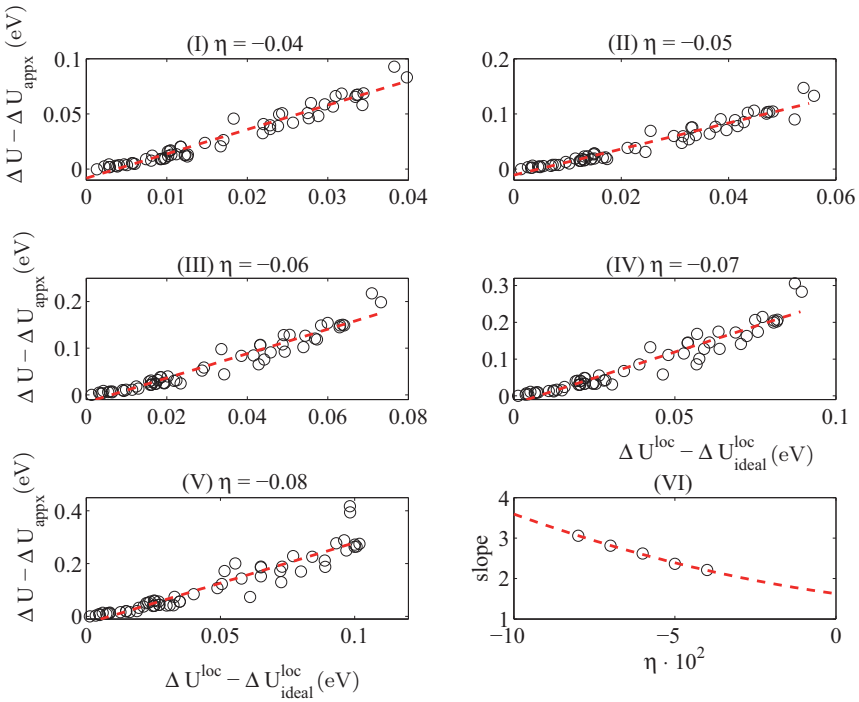

FIG. 4. (I)–(V) *are plots of the global distortion versus the local distortion for different misfits. The data are shown as (o) and the best fitting line is shown as (- -). Plot* (VI) *fits a quadratic curve to the relationship between the misfit and the slope of the best fitting line.*

3.4. The algorithm. We now give an overview of the full KMC algorithm.

1. Perform a global relaxation, detect the surface atoms (coordination number less than five), and compute hopping rates as discussed in subsection 3.3.
2. Compute the partial sums $p_j = \sum_{k=1}^{j} R_k$ and the total rate $R_{\text{total}} = R_d + \sum_{k=1}^{N} R_k$.
3. Select a surface atom or deposition event using p_j.
4. Move the selected atom (either a hopping or deposition event) using the method outlined in subsection 3.1.
5. Attempt a local relaxation; if this is not successful, perform a global one.
6. Update the rates of the atoms that were relaxed.
7. Perform a global update every N_G steps.
8. Return to step 2.

4. Results. In this section we present results from our simulations in a variety of situations.

4.1. Bilayer bending. As a check of the nonlinear conjugate gradient algorithm (i.e., the global relaxation scheme), we run tests to capture the predictions of Stoney's formula [9]: that the curvature, κ, of a thin film bilayer under external stress is given by

$$\kappa = C\frac{\eta}{{h_s}^2}, \tag{4.1}$$

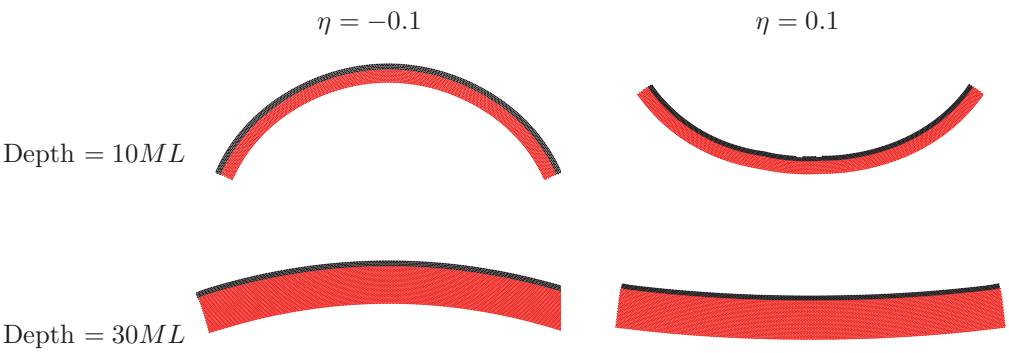

FIG. 5. *Stressed elastically strained system after relaxation with* $\eta \in \{-0.1, 0.1\}$.

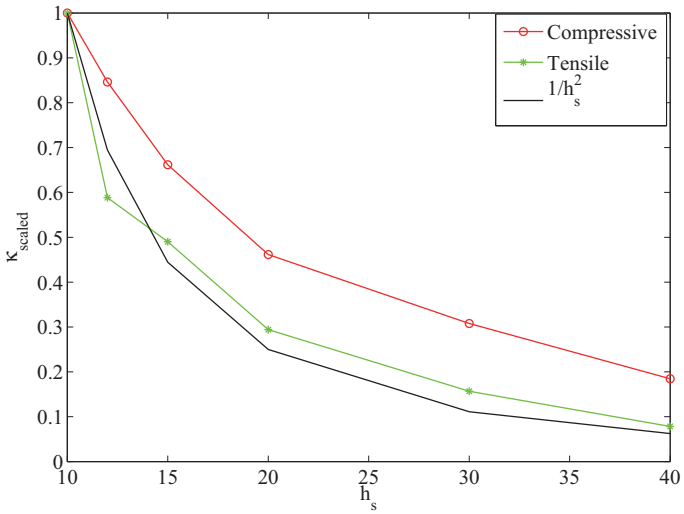

FIG. 6. *A plot of scaled film curvature for different substrate depths* h_s.

where C is a positive constant which depends on the height of the film and the biaxial elastic moduli of the film and substrate, and h_s is the depth of the substrate. The formula predicts that the curvature will be convex with a compressive misfit, $\eta < 0$, and concave with a tensile misfit, $\eta > 0$. We tested the code by relaxing 3 ML of film on substrates with different depths with the system squeezed in order to generate an external stress. The squeeze was implemented by constraining the width of the system to a slightly smaller length than was natural. In Figure 5, the first column is for a compressive misfit $\eta = -0.1$ and the second column is for a tensile misfit, $\eta = 0.1$. As expected the curvatures in the first column are convex and those in the second column are concave. In addition, in both the compressive and tensile regimes, the curvature decreases with increasing substrate depth, h_s. Figure 6 is a plot of curvature for different substrate depths for both compressive and tensile strains. Each graph is scaled by the largest curvature, i.e., the curvature for $h_s = 10$ ML, and each qualitatively follows the $1/h_s^2$ dependence predicted by Stoney's formula, (4.1).

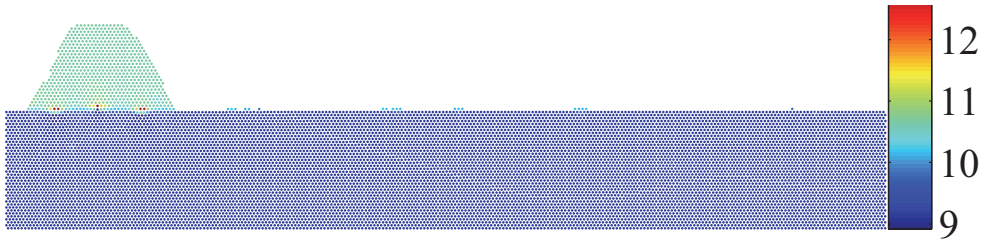

FIG. 7. *The configuration after annealing* 4 *ML of film on* 40 *ML of substrate with* $\eta = -0.08$. *Atoms are colored by the square of their average distance from nearest neighbors.*

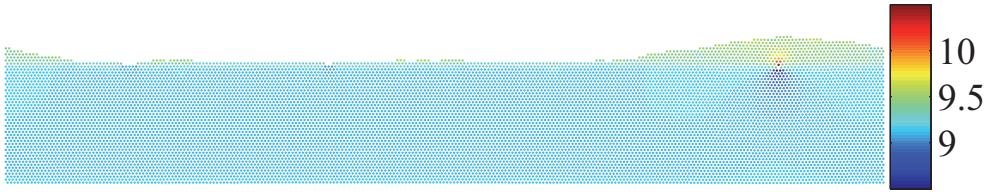

FIG. 8. *The configuration after annealing* 4 *ML of film on* 40 *ML of substrate with* $\eta = -0.02$. *Atoms are colored by the square of their average distance from nearest neighbors.*

4.2. Annealing. Consider the situation of a 4 ML flat film of material A on a substrate of material B. We examine two cases, one with high misfit, $\eta = -0.08$, and one with small misfit, $\eta = -0.02$. Both the film and substrate were 256 atoms wide. In the case with $\eta = -0.08$ the film forms an island with no appreciable wetting layer and several edge dislocations. The resulting configuration is shown in Figure 7. The film atoms are green and the substrate atoms are blue. For the case $\eta = -0.02$, the film also rearranges to form an island, but in this case a wetting layer has also formed Figure 8. The time scales reached depend on the misfit. For example, Figure 7 was observed in 2.3 million steps, which was 63 seconds in physical time. Conversely, Figure 8 took 63 million steps, which in physical time was 1824 seconds. In these figures, the atoms are colored by the square of the average distance from nearest neighbors. Dislocations are present at regions where the atoms are colored differently from neighboring atoms. We further explain our approach for detecting dislocations in the next section.

4.3. Detection and characteristics of edge dislocations. We detect dislocations or vacancies in our configurations in two ways. One way is to color each atom by the square of the average of its distance from nearest neighbors that lie within a radius of $1.15\sigma_A$. Atoms at a dislocation will have a significantly larger separation from their nearest neighbors than the surrounding atoms and thus will be colored differently. The second way is to color each atom by its total energy. Since the atoms at the dislocation will be higher in energy compared to the atoms around it, they will be colored differently.

Figure 8 shows the annealed system with each atom colored by the square of the average of its distance from nearest-neighbor atoms. Since substrate atoms have a smaller natural lattice spacing than the film atoms, the square of their average distance from nearest neighbors is smaller than that of the film atoms. In the figure, the substrate atoms are colored blue and the film atoms are colored green. The spots of blue in the film indicate the presence of substrate atoms in the film due to intermixing.

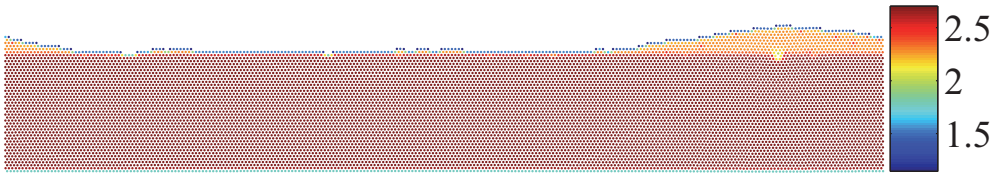

FIG. 9. *The configuration after annealing* 4 *ML of film on* 40 *ML of substrate with* $\eta = -0.02$. *Atoms are colored by the absolute value of their energies.*

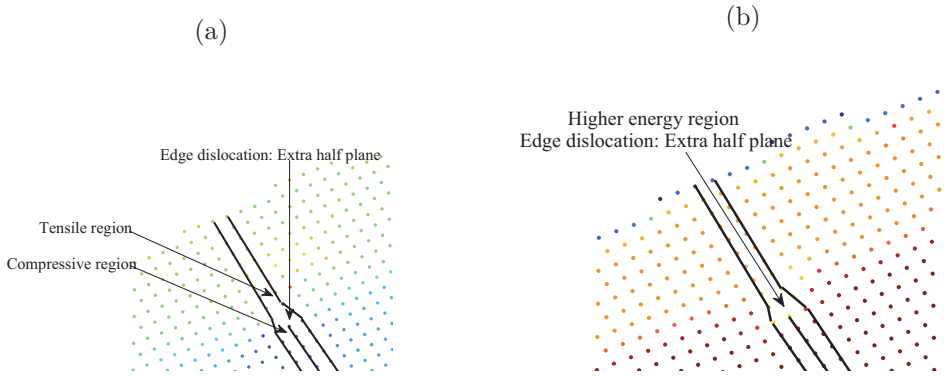

FIG. 10. *A closeup of the dislocation shown in Figure* 9 *with atoms colored by the square of their average distance from nearest neighbors* (a)*, and by the absolute value of their energy* (b).

The region in the bulk with a different color (yellow) from the neighboring region indicates the presence of a dislocation. The island grows over the dislocation because the strain due to mismatch is most relaxed at the dislocation [9].

In Figure 9, the atoms are colored by the absolute value of their energies due to the other atoms. The energies are all negative, so a high absolute value indicates a lower energy atom. The figure shows, as expected, that the substrate atoms have lower bond energies than the film atoms. The atoms on the surface have higher energies because of their low coordination number. The dislocation is colored yellow and surrounded by orange colored film atoms.

Figure 10(a) provides a closer view of the dislocation detected by coloring each atom by the square of its average distance from nearest neighbors. The figure is generated by a three-dimensional (3D) scatter plot where the y-coordinates are set to zero and the x- and z-coordinates are the coordinates of the atoms in $(1 + 1)$-dimension. The figure is rotated in order to detect the presence of the extra half plane which is characteristic of an edge dislocation. The azimuthal rotation is 37.5° clockwise at an elevation of 30.0°, which is the default 3D view in MATLAB. From the coloring scheme, we see that the atoms in the region right below the dislocation, where the extra half plane is present, have smaller separations from their neighbors, indicating a compressive region. On the other hand, the atoms in the region above the dislocation, where there is no half plane, have a larger separation from their neighbors. This is the tensile region. This observation has been presented in many texts (e.g., [5, 9]). Figure 10(b) is a closer look at the edge dislocation, revealing the presence of the extra half plane and the higher energy of the atoms at the dislocation.

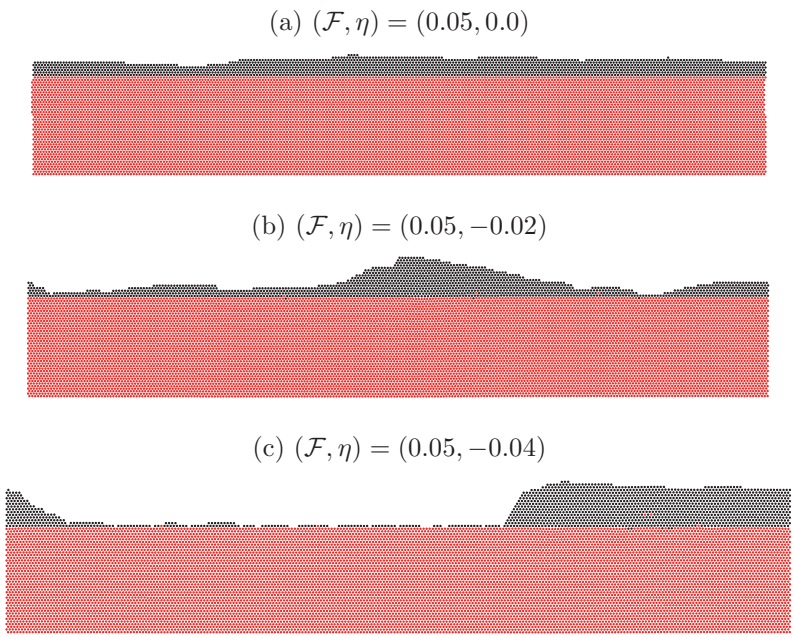

FIG. 11. 6 *ML of film deposited on* 40 *ML of substrate with a deposition flux,* $\mathcal{F}$*, of* 0.05 *ML/sec and at different misfits,* η*. The substrate atoms are light (red) and the film atoms are dark (black). Plots* (a), (b)*, and* (c) *correspond to* 0%*,* 2%*, and* 4% *misfit, respectively. They show a change in the growth pattern from Frank–van der Merwe (FM),* $\eta = 0.0$*, to Stranski–Krastanov (SK),* $\eta = -0.02$*, to Volmer–Weber (VW),* $\eta = -0.04$*.*

4.4. Dependence of growth modes on misfit strength. To verify that our method captures the *Frank–van der Merwe* (FM), *Stranski–Krastanov* (SK), and *Volmer–Weber* (VW) growth modes, we performed KMC simulations with misfits $\eta \in \{0.00, -0.02, -0.04\}$, temperature $T = 600K$, and flux $\mathcal{F} = 0.05$ ML/sec. In all the runs the substrate was 256 atoms wide and 40 monolayers deep. We applied periodic boundary conditions in the horizontal direction. We note that, unlike [19, 4, 20], we do not follow our deposition with an annealing run.

Figure 11 shows the results of the KMC simulations for all three misfits after deposition of 6.0 monolayers of the film. The substrate atoms are light (red) and the film atoms are dark (black). Figures 11(a), (b), and (c) have misfits of 0.00, -0.02, and -0.04, respectively. We see a change in the growth mode from layer-by-layer (FM) in (a), to island-on-layer (SK) in (b), and finally to island growth (VW) in (c).

The growth mode is governed by the competition between surface energy and elastic strain due to the size of the misfit. In the no misfit case, (a), there is an absence of elastic strain, and hence the film grows layer-by-layer in order to minimize surface energy. For $\eta = -0.02$, surface energy dominates until a wetting layer forms; then elastic strain dominates because the film adopts the crystal structure of the substrate [9]. Then deposition proceeds via island growth on the wetting layer in order to minimize the strain leading to island-on-layer growth. When $\eta = -0.04$, elastic strain dominates from the onset of deposition and the film forms islands, without wetting the surface, in order to minimize the strain at the cost of higher surface energy.

A close examination of Figure 11 reveals that more dislocations are formed at higher misfit. To make this more apparent we plot Figure 12, which shows no dislo-

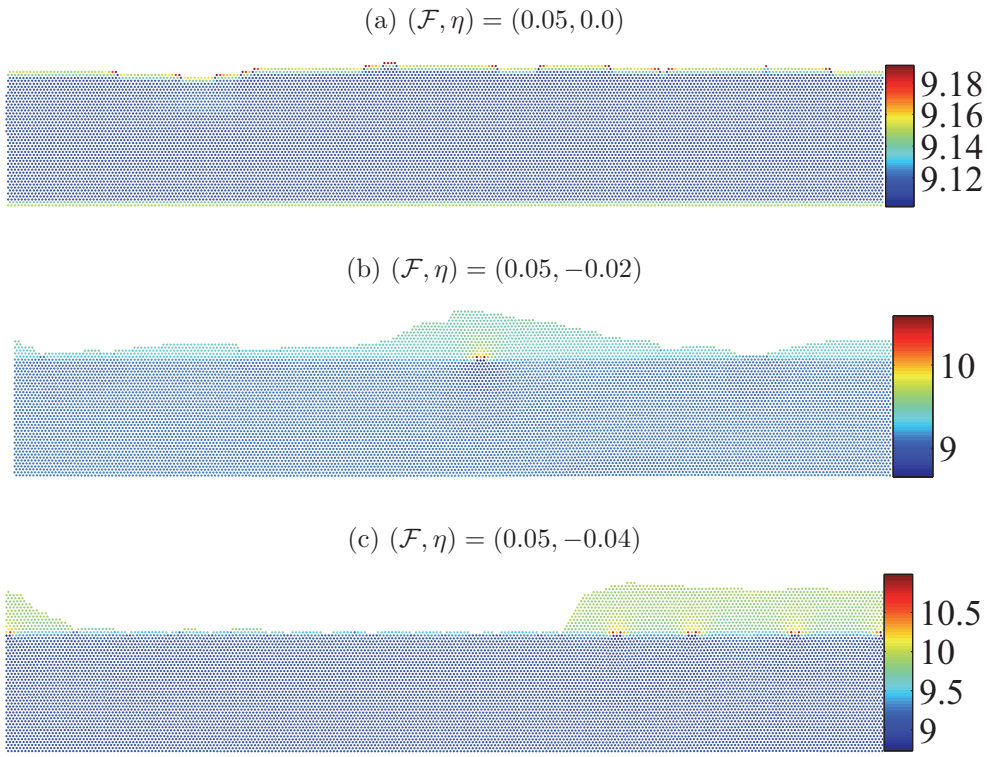

FIG. 12. 6 *ML of film deposited on* 40 *ML of substrate with a deposition flux,* $\mathcal{F}$*, of* 0.05 *ML/sec and at different misfits,* η*. Plots* (a), (b), *and* (c) *correspond to* 0%, 2%, *and* 4% *misfit, respectively. No dislocations are formed in* (a) *with* $\eta = 0.0$*, one dislocation is formed in* (b), $\eta = -0.02$*, and four dislocations are formed in* (c), $\eta = -0.04$.

cation for the no misfit case, (a), a single dislocation for case (b), $\eta = -0.02$, and four dislocations for case (c) where $\eta = -0.04$.

4.5. Effect of flux (deposition rate) on island formation. Next, we examine the effect of the deposition rate on island formation by performing simulations with misfit, $\eta = -0.04$, and flux, $\mathcal{F} \in \{0.5, 0.125, 0.05\}$ at $T = 600K$. Figures 13(a), (b), and (c) correspond to deposition rates of 0.5, 0.125, and 0.05 monolayers per second, respectively. As pointed out in [21], lower deposition rates promote island formation. Because of the increase in hopping frequency between depositions, the adatoms are able to drift and combine with previously nucleated islands to form larger islands. Multilayered islands can be energetically preferred over flat films in the presence of strain since they can more easily reduce their strain energy [21, 3, 10]. Figure 13 shows that as the deposition flux is reduced, the number of islands decreases and the island size gets larger. Additionally, higher deposition flux leads to the formation of more dislocations.

4.6. Anticorrelation of quantum dots on opposite sides of a film. Finally, we briefly consider the growth of film on both sides of a substrate. Our approximate off-lattice KMC appears to support experimental findings reported in [15]. Deposition and annealing simulations analogous to the experiments described in [15] capture anticorrelation of quantum dots on opposite sides of the substrate. In the first example,

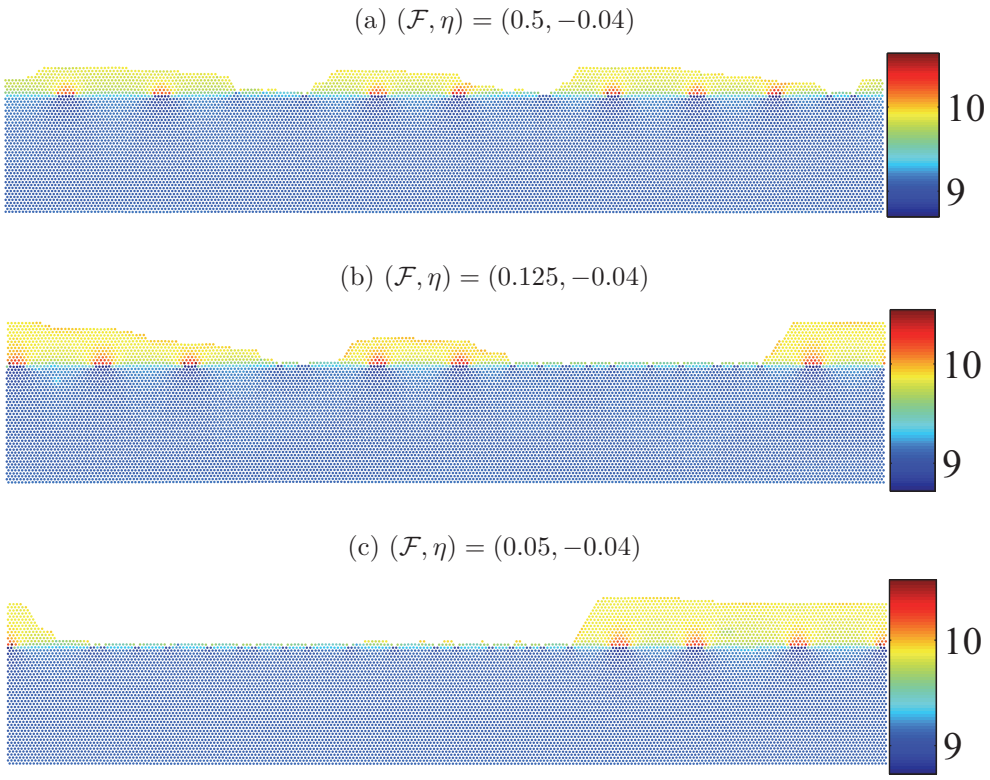

FIG. 13. *6 ML of film deposited on 40 ML of substrate with misfit* $\eta = -0.04$ *and different fluxes,* $\mathcal{F}$. *Plots* (a), (b), *and* (c) *correspond to* 0.5, 0.125, *and* 0.05 *ML/sec, respectively. A lower flux leads to more hopping and fewer, but larger, islands.*

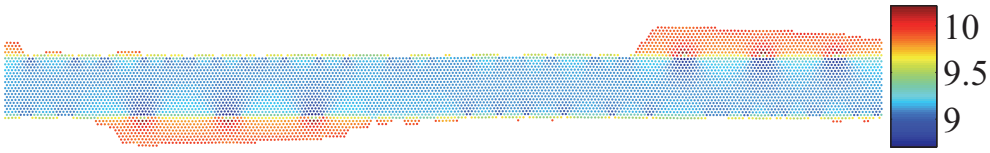

FIG. 14. *The figure shows anticorrelated quantum dots formed as a result of deposition on both sides of a 20 ML substrate at* $(\mathcal{F}, \eta) = (0.05, -0.04)$.

we deposited film atoms on both sides of 20 monolayers of substrate at $T = 600K$ with $(\mathcal{F}, \eta) = (0.05, -0.04)$. The result is shown in Figure 14. It is suggested in [15] that when a Ge quantum dot forms on one side of the substrate, it creates tensile strain in the substrate region right below the quantum dot, which in turn creates a compressive strain in the substrate region at the opposite surface. The compressive strain on this opposite surface is a slight barrier to formation of a Ge quantum dot. As a result, the Ge atoms on this surface form quantum dots in a region of tensile strain. This pattern repeats, leading to a periodic array of anticorrelated quantum dots on opposite sides of the film. However, the story may be more complicated than this since it is well established both experimentally and theoretically that elastic interactions are responsible for the alignment of stacked quantum dots (e.g., [27]).

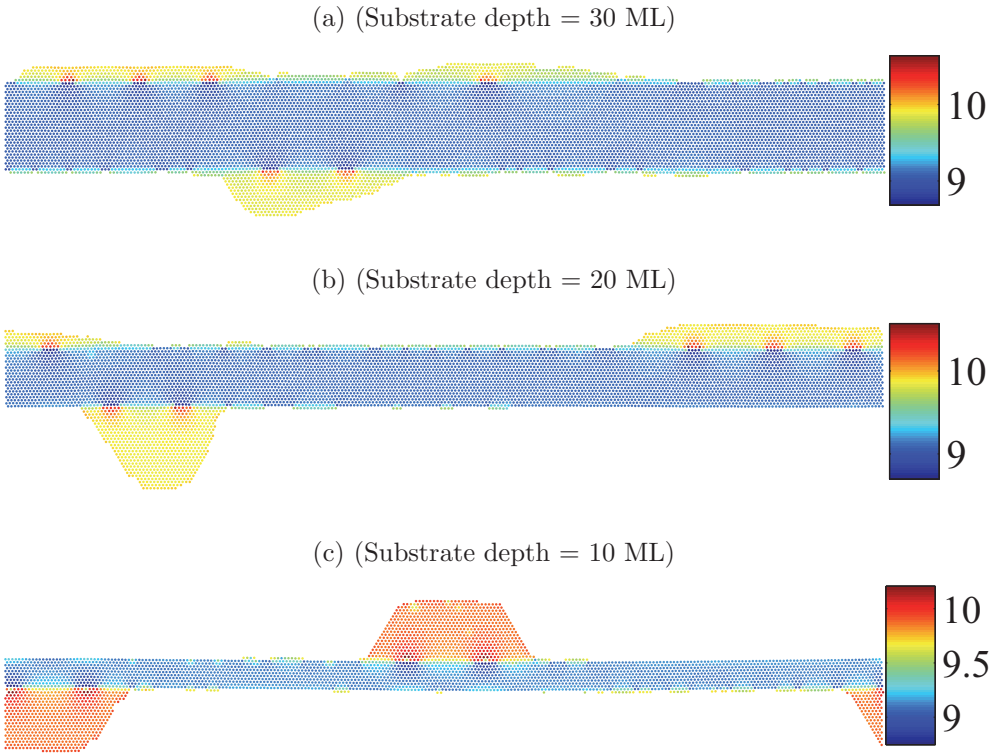

FIG. 15. *Annealing of configurations with three monolayers of film on either side of a substrate. Plots* (a), (b), *and* (c) *correspond to substrate depths of* 30, 20, *and* 10 *monolayers. Anticorrelation in the quantum dots is most prominent in* (c) *where the substrate depth is smallest.*

In the second example, we annealed substrates of different depths, each sandwiched by 3 ML of film on both sides, with misfit $\eta = -0.04$ at $T = 600K$. Figure 15 shows the results, with plots (a), (b), and (c) corresponding to substrate depths of 30, 20, and 10 ML, respectively. The strength of the anticorrelation of the quantum dots decreases with increasing depth. Our KMC method captures this dependence, which was also observed experimentally in [15]. For thicker substrates the effect of the strain from one side on the opposite side is lower. As such, the kinetics on one side proceeds with little to no effect from the opposite side.

5. Conclusion. In this paper, we have introduced an approximate off-lattice kinetic Monte Carlo method to model heteroepitaxial growth. We have shown that the method captures the dependence of the growth modes on the misfit strain, the dependence of island formation on the deposition flux, and the anticorrelation of quantum dots grown on both sides of a substrate. The method nucleates dislocations, a feature absent in solid-on-solid models. It naturally incorporates intermixing, is relatively easy to implement, and offers a fast method for gaining a qualitative understanding of many physical phenomena in crystal growth.

Acknowledgments. The computations were performed on the University of Michigan SCREMS computing cluster. We thank Joanna Millunchick for helpful conversations concerning dislocations and Ken Elder for suggesting the problems on anticorrelated growth during the IPAM long program on Materials Defect: Mathematics, Computation, and Engineering.

REFERENCES

[1] M. P. Allen and D. J. Tildesley, *Computer Simulation of Liquids*, Oxford University Press, New York, 1987.

[2] A. Baskaran, J. Devita, and P. Smereka, *Kinetic Monte Carlo simulation of strained heteroepitaxial growth with intermixing*, Continuum Mech. Thermodyn., 22 (2010), pp. 1–26.

[3] P. Berger, K. Chang, P. K. Bhattacharya, and K. K. Bajaj, *Role of strain and growth conditions on the growth front profile of In_x on GaAs during the pseudomorphic growth regime*, Appl. Phys. Lett., 53 (1988), pp. 684–686.

[4] M. Biehl, M. Ahr, W. Kinzel, and F. Much, *Kinetic Monte Carlo simulations of heteroepitaxial growth*, Thin Solid Films, 428 (2003), pp. 52–55.

[5] W. D. Callister, *Materials Science and Engineering: An Introduction*, 8th ed., John Wiley & Sons, New York, 2010.

[6] S. Clarke and D. D. Vvedensky, *Growth kinetics and step density in reflection high-energy electron diffraction during molecular-beam epitaxy*, J. Appl. Phys., 63 (1988), pp. 2272–2283.

[7] B. W. Dodson and P. A. Taylor, *Monte Carlo simulation of continuous-space crystal growth*, Phys. Rev. B, 34 (1986), pp. 2112–2115.

[8] D. Frenkel and B. Smit, *Understanding Molecular Simulation: From Algorithms to Applications*, 2nd ed., Academic Press, New York, 2001.

[9] L. B. Freund and S. Suresh, *Thin Film Materials*, Cambridge University Press, Cambridge, UK, 2003.

[10] M. H. Grabow and G. H. Gilmer, *Molecular dynamics studies of semiconductor thin films and interfaces*, Mat. Res. Soc. Symp. Proc., 94 (1987), pp. 15–24.

[11] W. Guo, T. P. Schulze, and W. E, *Simulation of impurity diffusion in a strained nanowire using off-lattice KMC*, Comm. Comput. Phys., 2 (2007), pp. 164–176.

[12] G. Henkelman and H. Jonsson, *Improved tangent estimate in the nudged elastic band method for finding minimum energy paths and saddle points*, J. Chem. Phys., 113 (2000), pp. 9978–9985.

[13] G. Henkelman and H. Jonsson, *Long time scale kinetic Monte Carlo simulations without lattice approximation and predefined event table*, J. Chem. Phys., 115 (2001), pp. 9657–9666.

[14] G. Henkelman, B. P. Uberuaga, and H. Jonsson, *A climbing image nudged elastic band method for finding saddle points and minimum energy paths*, J. Chem. Phys., 113 (2000), pp. 9901–9904.

[15] S. Kwon, Z. C. Y. Chen, J.-H. Kim, and J. Xiang, *Misfit-guided self-organization of anticorrelated Ge quantum dot arrays on Si nanowires*, Nano Lett., 12 (2012), pp. 4747–4762.

[16] C. H. Lam, C. K. Lee, and L. M. Sander, *Competing roughening mechanisms in strained heteroepitaxy: A fast kinetic Monte Carlo study*, Phys. Rev. Lett., 89 (2002), 216102.

[17] A. C. Levi and M. Kotrla, *Theory and simulation of crystal growth*, J. Phys. Condens. Matter, 9 (1997), pp. 299–344.

[18] M. T. Lung, C. H. Lam, and L. M. Sander, *Island, pit, and groove formation in strained heteroepitaxy*, Phys. Rev. Lett., 95 (2005), 086102.

[19] F. Much, M. Ahr, M. Biehl, and W. Kinzel, *A kinetic Monte Carlo method for the simulation of heteroepitaxial growth*, Comput. Phys. Comm., 147 (2002), pp. 226–229.

[20] F. Much and M. Biehl, *Simulation of wetting-layer and island formation in heteroepitaxial growth*, Europhysics Lett., 63 (2003), pp. 14–20.

[21] B. G. Orr, D. A. Kessler, C. W. Snyder, and L. M. Sander, *A model for strain-induced roughening and coherent island growth*, Europhysics Lett., 19 (1992), pp. 33–38.

[22] G. Russo and P. Smereka, *Kinetic Monte Carlo simulations of strained epitaxial growth in three dimensions*, J. Comput. Phys., 214 (2006), pp. 809–828.

[23] G. Russo and P. Smereka, *A multigrid-Fourier method for the computation of elastic fields with application to heteroepitaxy*, Multiscale Model. Simul., 5 (2006), pp. 130–148.

[24] M. Schroeder and D. E. Wolf, *Diffusion on strained surfaces*, Surf. Sci., 375 (1997), pp. 129–140.

[25] T. P. Schulze and P. Smereka, *An energy localization principle and its application to fast kinetic Monte Carlo simulation of heteroepitxatial growth*, J. Mech. Phys. Sol., 3 (2009), pp. 521–538.

[26] T. P. Schulze and P. Smereka, *Simulation of three-dimensional strained heteroepitaxial growth using kinetic Monte Carlo*, Comm. Comput. Phys., 10 (2011), pp. 1089–1112.

[27] T. P. Schulze and P. Smereka, *Kinetic Monte Carlo simulation of heteroepitaxial growth: Wetting layers, quantum dots, capping, and nanorings*, Phys. Rev. B, 86 (2013), 235313.

[28] J. R. Shewchuk, *An Introduction to the Conjugate Gradient Method without the Agonizing Pain*, Tech. report, School of Computer Science, Carnegie Mellon University, Pittsburgh, PA, 1994.

[29] P. Smilauer and D. D. Vvedensky, *Coarsening and slope evolution during unstable epitaxial growth*, Phys. Rev. B, 52 (1995), pp. 14263–14272.

[30] M. R. Sørensen and A. F. Voter, *Temperature-accelerated dynamics for simulation of infrequent events*, J. Chem. Phys., 112 (2000), pp. 9599–9606.

[31] A. F. Voter, *Hyperdynamics: Accelerated molecular dynamics of infrequent events*, Phys. Rev. Lett., 78 (1997), pp. 3908–3911.

[32] A. F. Voter, *A method for accelerating the molecular dynamics simulation of infrequent events*, J. Chem. Phys., 106 (1997), pp. 4665–4677.

[33] A. F. Voter, *Parallel replica method for dynamics of infrequent events*, Phys. Rev. B, 57 (1998), pp. R13985–R13988.

[34] A. F. Voter, F. Montalenti, and T. C. Germann, *Extending the time scale in atomistic simulation of materials*, Ann. Rev. Mater. Res., 32 (2002), pp. 321–346.